Extended Abstracts of the 2013 International Conference on Solid State Devices and Materials, Fukuoka, 2013, pp1156-1157

Impurities distribution and recombination activity in as-grown and annealed multicrystalline silicon

Takuto Kojima[1], Tomihisa Tachibana[1], Nobuaki Kojima[1], Yoshio Ohshita[1] Koji Arafune[2], Atsushi Ogura[3] and Masafumi Yamaguchi[1,]

[1] Toyota Tech. Inst.
2-12-1 Hisakata, Tempaku-ku, Nagoya, Aichi 468-8511, Japan
Phone: +81-52-809-1830 E-mail: sd12501@toyota-ti.ac.jp
[2] Univ. Hyogo
2167 Shosha, Himeji, Hyogo 671-2201, Japan
[3] Meiji Univ.
1-1-1 Higashi-Mita, Tama-ku, Kawasaki-shi, Kanagawa 214-8571, Japan

Abstract

To study the impact of annealing on the impurities distribution and the recombination activity of multicrystalline silicon, the synchrotron-based x-ray analysis, the electron beam induced current, and the photoluminescence mapping of near band edge and 0.78 eV deep emission were performed before and after annealing. Nickel agglomerates existed along random grain boundaries; while not along most of coincidence cite lattice grain boundaries (Σ3, Σ 9 and Σ 27a) and some of random grain boundaries. At most of the recombination active grain boundaries, the existence of nickel agglomerates was indicated.

1. Introduction

Multicrystalline silicon grown by cast method has been playing an important role in PV market for the decade due to the well balanced cost and efficiency. Today, further cost reduction is expected by using less pure silicon feedstock, that is, solar grade silicon [1-6]. Solar grade silicon cannot avoid incorporation of relatively high concentration of metal species, and it is well known that some metal species drastically deteriorates conversion efficiency [7-9]. Iron, copper and nickel have been given special attention due to the impact on solar efficiency and diffusivity in silicon matrix under thermal process. The distribution of iron, copper and nickel in multicrystalline silicon has been studied using synchrotron based X-ray technique at ALS in U.S. [10-14], BESSY-II in Germany [15-17], SPring-8 in Japan [18, 19]. The metals distribute as atomically dissolved states, nanometers silicide particles, and micrometers inclusions including metal oxide [10, 13] Nickel and copper mainly segregates at grain boundaries (GBs) due to high diffusivity, which induces recombination activity at GBs [11, 13]. The recombination activities of intentionally iron-incorporated GBs have been studied by electron beam induced current (EBIC) method [20-23]. On the other hand, recombination activity of GBs without intentional metal contamination has not been adequately studied. In this study, relation between nickel distribution, recombination activity, and crystallographic structure of GBs before and after thermal process using synchrotron-based x-ray fluorescence microscopy (μ-XRF), electron beam induced current (EBIC) method, and electron back scatter diffraction pattern (EBSD) method.

2. Experimental

Ga doped mc-Si ingot was grown by unidirectional cast method using off-specification of electronics grade polycrystalline silicon as feedstock The grown ingot was cylindrical-shaped with a diameter and a height of approximately 100 mm, and was sliced into 300-μm-thick substrates. To compare effects of annealing temperatures, three adjacent substrates were used in this study. The set of substrates were selected from the upper part of the ingot with a fraction solidified ~0.85, where concentration of impurities is relatively high due to segregation phenomena. The concentrations of impurities were measured using the inductively coupled plasma mass spectrometer (ICP-MS) and atomic absorption spectrometry (AAS) methods. The average iron, copper and nickel concentrations were 3.5×10^{13}, 1.0×10^{14}, and 3.3×10^{14} atoms/cm^3, respectively. The first substrate was left unprocessed, and the second and third substrates were subjected to thermal treatment at 650 ºC for 120 min and 1000 ºC for 90 min with an N_2 ambient, respectively. The crystallographic orientation was analyzed by scanning electron microscope equipped with a TSL EBSD pattern collection system. The distributions of transition metals and their chemical states in the substrates were studied using synchrotron-based measurements at the beam line 37XU in SPring-8. The distribution was analyzed by the μ-XRF mapping with an energy of 10 keV, a beam size of 0.7 x 1.5 μm and a sampling pitch of 5 μm. The recombination activity was characterized by the EBIC measurements on the aluminum Schottky carrier separation.

3. Results and Discussion

XRF mappings for nickel signal and EBIC images of the unprocessed, 650 °C annealed, and 1000 °C annealed samples were shown in Fig. 1 (a) and (b), respectively. The position of observed region is identical to each sample in

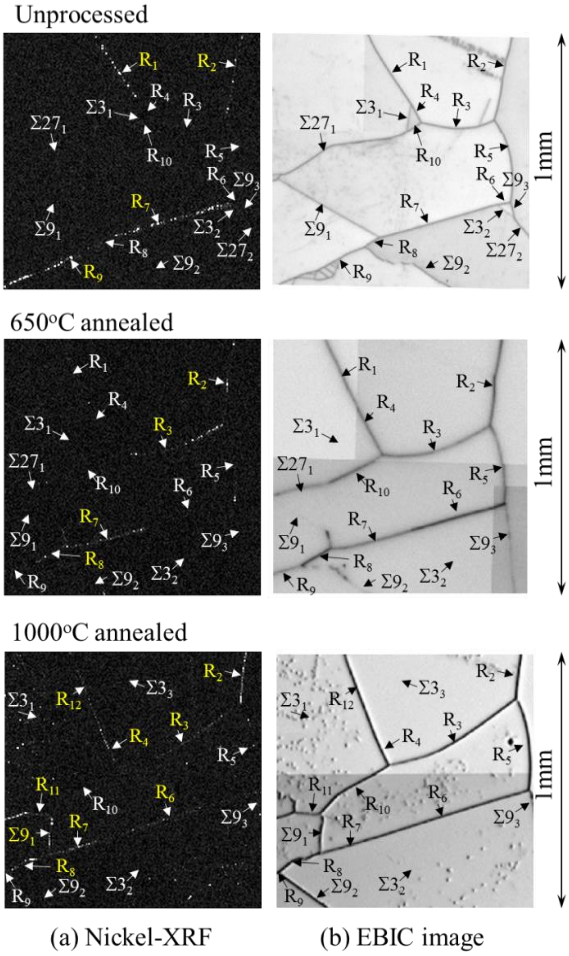

Fig. 1 (a) Nickel signal map in XRF measurement and (b) EBIC image for the same location of XRF maps.

the surface vertical to growth direction. The signs in the figure indicates GB structures analyzed by EBSD, which indicates random angle boundaries (labeled 'R') and coincide site lattice (CSL) boundaries (labeled 'Σ + index'), and the subscripts were added to the labels to identify GBs. GBs with the same symbol in different samples are identical. Nickel signal in μ-XRF distributes only at GBs for unprocessed and 650 °C annealed samples. For 1000 °C annealed sample, nickel signal was observed at GBs and intra grain. In the unprocessed sample, all the GBs in the measured region indicated EBIC contrast. By thermal process, EBIC contrast disappeared at most of CSL GBs, while at random GBs EBIC contrast remained. By 1000 °C annealing, there are spot-like EBIC contrast at the intra grain position like nickel XRF signal.

Comparing different thermal processes, random GB R_2 and R_7 indicated nickel XRF signal and EBIC contrast before and after two thermal processes. GBs other than R_2 and R_7 indicated and did not indicate nickel distribution and EBIC contrast, and R_9 indicated no nickel signal in the three samples. GBs with nickel signal accompanied EBIC contrast, but not necessarily vice versa. R_6 after 650 °C annealing especially indicated strong EBIC contrast, but no nickel signal.

In summary, nickel dramatically redistributes by thermal process at as low temperature as 650 °C. Nickel does not redistribute at most CSL GBs and some specific random GBs. At some GBs, nickel segregates after one annealing but not the other annealing. There are GBs indicating EBIC contrast without nickel, so recombination activity is not necessarily related to nickel distribution. The different metal capture and release activity of random GBs is to be studied.

4. Conclusion

Effects of annealing at low and high temperatures on nickel distribution and GBs recombination activity was studied by synchrotron-based x-ray analysis and EBIC. Nickel differently redistributes by different thermal conditions. Recombination activity is not necessarily related to nickel distribution.

Acknowledgements

Part of this study was supported by New Energy and Industrial Technology Development Organization (NEDO). We would like to express sincere thanks to all the contributors to the Conference for their cooperation in the Conference program. The authors would like to thank Yasuko Terada of JASRI for their technical cooperation.

References

[1] A. A. Istratov *et al.*.: Mater. Sci. Eng. B **134** (2006) 282.
[2] A. F. B. Braga *et al.*.: Sol. Ener. Mater. Sol. Cells **92** (2008) 418.
[3] S. Pizzini: Sol. Ener. Mater. Sol. Cells **94** (2010) 1528.
[4] C. Modanese *et al.*.: Prog. Photovolt. Res. Appl. **19** (2011) 45.
[5] V. Osinniy *et al.*.: Sol. Ener. Mater. Sol. Cells **95** (2011) 564.
[6] J. Safarian *et al.*.: Energy Procedia **20** (2012) 88.
[7] A. A. Istratov and E. R. Weber: Appl. Phys. A **66** (1998) 123.
[8] A. A. Istratov *et al.*.: Appl. Phys. A **70** (2000) 489.
[9] D. Macdonald and L. J. Geerligs: proc. of 19th European Solar Energy Conference (2004, Paris, France) 492.
[10] T. Buonassisi *et al.*.: Nature Materials **4** (2005) 676.
[11] T. Buonassisi *et al.*.: Appl. Phys. Lett. **87** (2005) 121918.
[12] T. Buonassisi *et al.*.: J. Appl. Phys. **97** (2005) 063503.
[13] T. Buonassisi *et al.*.: Prog. Photovolt. Res. Appl. **14** (2006) 513.
[14] T. Buonassisi *et al.*.: Appl. Phys. Lett. **89** (2006) 042102.
[15] W. Seifert *et al.*.: Phys. Status Solidi C **6** (2009) 765.
[16] W. Seifert *et al.*.: 3rd Intenational Workshop on Crystalline Silicon Solar Cells, SINTEF/NTNU, Trondheim NORWAY, 3-5 June 2009.
[17] M. Trushin *et al.*.: Phys. Stat. Solidi C **6** (2009) 1868.
[18] K. Arafune *et al.*.: Physica B **376** (2006) 236.
[19] K. Arafune *et al.*.: Jpn. J. Appl. Phys. **45** (2006) 6153.
[20] J. Chen and T. Sekiguchi: Jpn. J. Appl. Phys. **46** (2007) 6489.
[21] J. Chen *et al.*.: Phys. Status Solidi C **4** (2007) 2908.
[22] J. Chen *et al.*.: Solid State Phenomena **156-158** (2010) 19.
[23] T. Sameshima *et al.*.: Appl. Phys. Express **5** (2012) 042301.